Supplementary Material

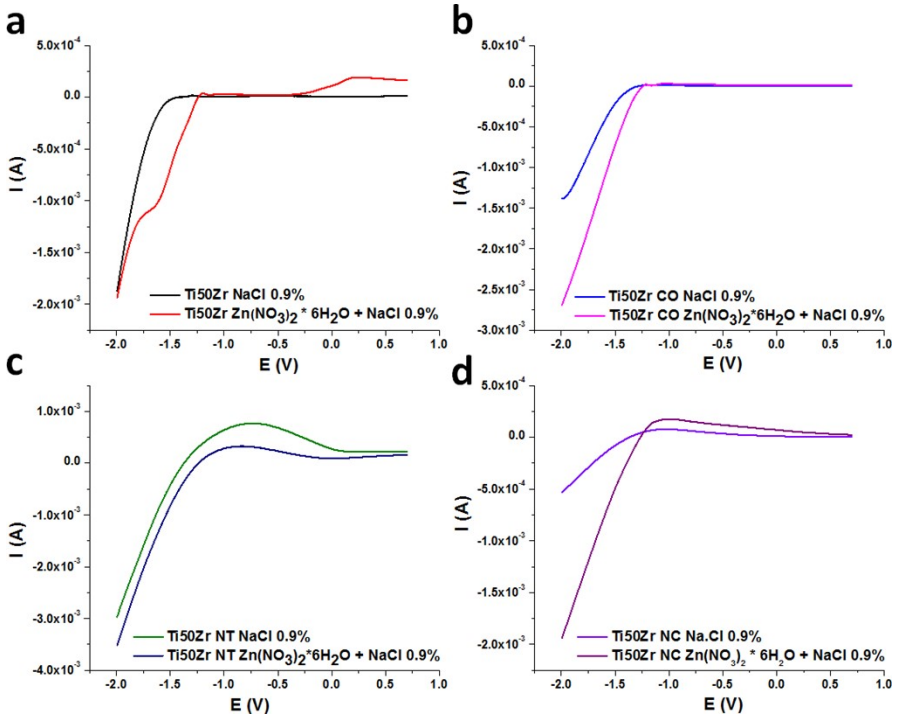

Figure S1. Cyclic voltammograms for Ti50Zr substrate and anodized samples in NaCl 0.9% and NaCl 0.9% +$Zn(NO_3)_2$.

Table S1. EDX results of Ti50Zr substrate and coated samples.

Sample	Element weight (%)			
	O	Zr	Ti	Zn
Ti50Zr	5.18	40.39	54.43	-
Ti50Zr ZnO	30.93	13.08	22.60	33.40
Ti50Zr CO	13.56	37.44	49.00	-
Ti50Zr COZnO	31.60	11.27	20.60	36.53
Ti50Zr NT	35.77	27.37	36.86	-
Ti50Zr NTZnO	34.55	27.11	35.37	2.97
Ti50Zr NC	35.10	27.74	37.17	-
Ti50Zr NCZnO	34.54	27.47	35.88	1.11

Optical band gap

From Tauc plots, E_g was determined by PE procedure to have more accurate results, Fig. S2.

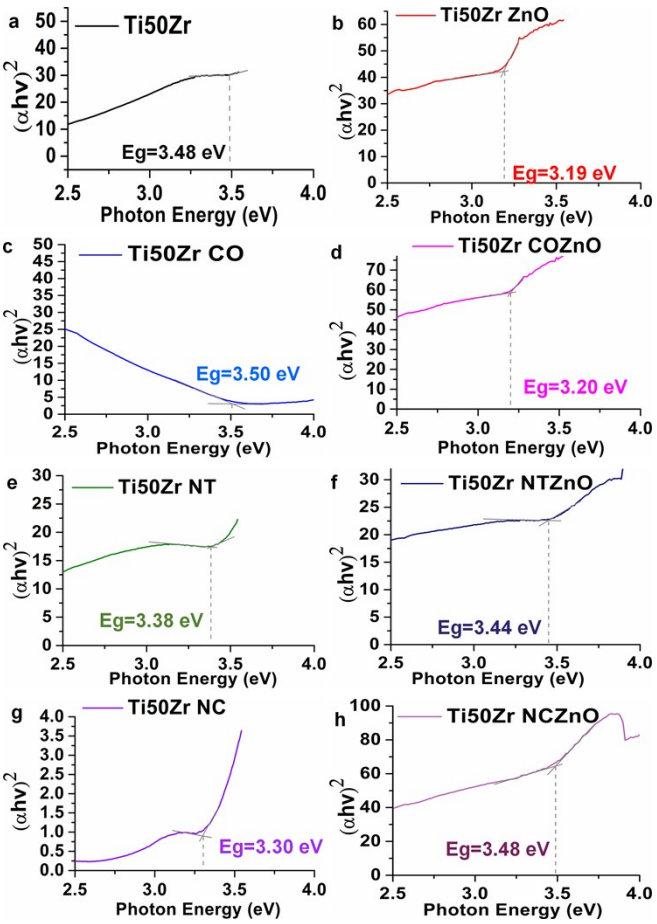

Figure S2. Tauc plots obtained from the optical transmittance spectra of a) Ti50Zr, b) Ti50Zr ZnO, c) Ti50Zr CO, d Ti50Zr COZnO, c) Ti50Zr NT and Ti50Zr NTZnO, d) Ti50Zr NC and Ti50Zr NCZnO.

The data in Table S2 highlights the interplay between the electronic properties, surface morphology, and ZnO nanoparticle characteristics in determining the antibacterial performance of Ti50Zr alloys. The calculated E_{VB} and E_{CB} values suggest that the ZnO-coated samples are capable of generating reactive oxygen species (ROS) under appropriate conditions:

- Valence band values (E_{VB}) for ZnO-coated surfaces range from 2.89 eV (Ti50Zr ZnO) to 3.12 eV (Ti50Zr NCZnO), allowing sufficient oxidative potential for generating hydroxyl radicals (•OH).

- Conduction band values (E_{CB}) are consistently negative (e.g., -0.34 eV for Ti50Zr NTZnO, -0.36 eV for Ti50Zr NCZnO), enabling superoxide radical ($O_2^{\bullet -}$) formation.

Despite this, the ROS contribution alone does not fully explain the antibacterial effects. For instance, Ti50Zr NTZnO, which shows a band gap of 3.44 eV, exhibits the most significant bacterial inhibition (+47%) due to the presence of small ZnO nanoparticles (10 nm), which enhances direct physical and chemical interactions with bacterial membranes.

In contrast, Ti50Zr NCZnO combines a high band gap (3.48 eV) with sharp nanochannel morphology, achieving a 75% inhibition rate, largely attributed to mechanical effects rather than ROS generation alone.

Table S2. Milliken electronegativity (χ), band gap (Eg) from Tauc plot and calculated E_{VB} and E_{CB}.

Sample	Eg (eV)	χ (eV)	E_{VB} (eV)	E_{CB} (eV)
Ti50Zr	3.48	5.89	3.13	-0.35
Ti50Zr ZnO	3.19	5.80	2.89	-0.29
Ti50Zr CO	3.50	5.89	3.14	-0.36
Ti50Zr COZnO	3.20	5.86	2.96	-0.24
Ti50Zr NT	3.38	5.89	3.08	-0.30
Ti50Zr NTZnO	3.44	5.88	3.10	-0.34
Ti50Zr NC	3.30	5.89	3.04	-0.26
Ti50Zr NCZnO	3.48	5.88	3.12	-0.36

This analysis underscores that while ROS generation is enabled by band-edge alignment, the antibacterial efficacy of these materials is primarily governed by synergistic effects of surface morphology, ZnO particle size, and band gap tuning.

Electrochemical stability

Electrochemical impedance spectroscopy (EIS)

Figure S3 compares the Nyquist diagrams for untreated Ti50Zr and coated samples.

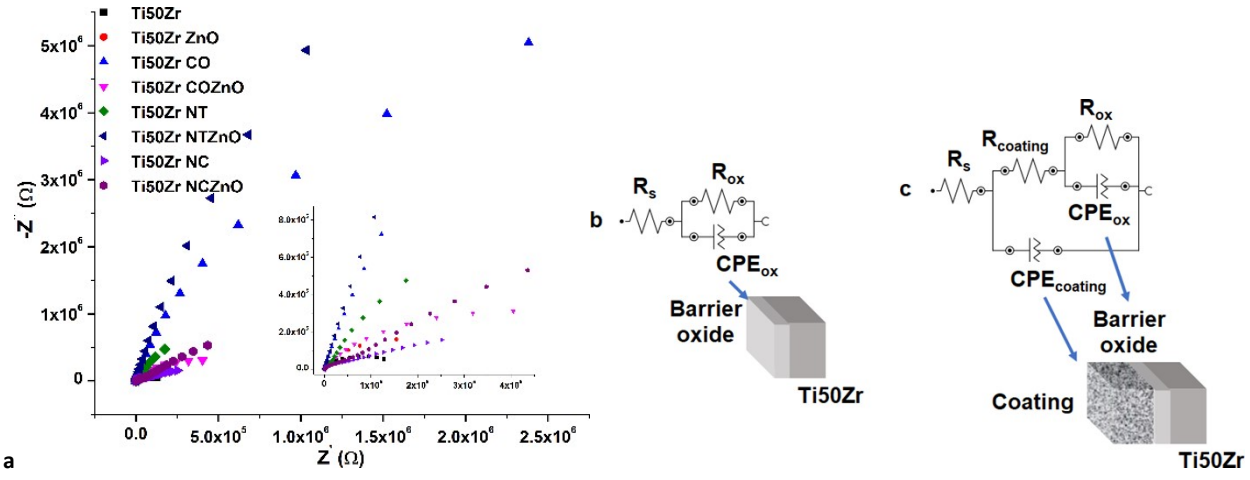

Figure S3. a) Nyquist diagrams for Ti50Zr substrate and coated sample, b) equivalent circuit used to fit the EIS data for untreated Ti50Zr and Ti50Zr CO c) equivalent circuit used to fit the EIS data for all other coated samples.

Figure S3 shows Nyquist diagrams for untreated Ti50Zr and coated samples, with two equivalent circuits used for data fitting. For untreated Ti50Zr and Ti50Zr CO, a simple modified Randles circuit was applied, accounting for the oxide layer's resistance (R_{ox}) and constant phase element (CPE). For coated samples, an additional coating resistance ($R_{coating}$) and $CPE_{coating}$ were included.
EIS analysis (Table S3) indicates that Rox values increase for anodized samples (Ti50Zr CO, NT, and NC), with Ti50Zr NT (closed-bottom nanotubes) showing higher resistance than Ti50Zr NC (open-bottom nanochannels). ZnO deposition on Ti50Zr and Ti50Zr CO reduces R_{ox}, likely due to oxide layer reduction during Zn electrodeposition. However, for nanostructured samples (NT, NC), Rox increases post-ZnO deposition, attributed to thermal treatment effects.
$R_{coating}$ values reflect surface structure, being lower for the porous NC oxide compared to NT nanotubes. Compact ZnO nanorods on Ti50Zr ZnO lead to higher $R_{coating}$ than the larger rods on Ti50Zr COZnO. Similarly, ZnO nanoparticles on Ti50Zr NTZnO and NCZnO increase $R_{coating}$, likely covering porous nanotube and nanochannel structures.
The pseudo-capacitive behavior of samples is evident from Nox values (0.80–0.98), except for Ti50Zr NC (N_{ox} = 0.50), indicating a less compact oxide layer. ZnO deposition improves Nox to ~0.70 due to reduced porosity from ZnO nanorods. Coating elements maintain $N_{coating}$ above 0.70 for all samples, reflecting consistent capacitive behavior.

Table S3. Values obtained from fitted EIS data using NOVA software.

Sample	R_S (Ω)	$R_{coating}$ (Ω)	$CPE_{coating}$		Rox	CPEox		χ^2
			Y_0 ($S \cdot s^n$)	N		Y_0 ($S \cdot s^n$)	N	
Ti50Zr	109.22	-	-	-	$0.02 \cdot 10^7$	$330 \cdot 10^{-7}$	0.88	0.006
Ti50Zr ZnO	140.95	$11 \cdot 10^4$	$9.30 \cdot 10^{-6}$	0.87	$0.003 \cdot 10^7$	$9 \cdot 10^{-7}$	0.80	0.05
Ti50Zr CO	96.64	-	-	-	$1.79 \cdot 10^7$	$15.4 \cdot 10^{-7}$	0.92	0.03
Ti50Zr COZnO	105.1	$4 \cdot 10^4$	$0.005 \cdot 10^{-6}$	0.88	$0.07 \cdot 10^7$	$48.2 \cdot 10^{-7}$	0.83	0.11
Ti50Zr NT	88.92	$8.45 \cdot 10^4$	$14.69 \cdot 10^{-6}$	0.88	$0.28 \cdot 10^7$	$85.0 \cdot 10^{-7}$	0.94	0.05
Ti50Zr NTZnO	80.70	$14.40 \cdot 10^4$	$2.42 \cdot 10^{-6}$	0.92	$5.58 \cdot 10^7$	$1.21 \cdot 10^{-7}$	0.98	0.05
Ti50Zr NC	137.33	$4.45 \cdot 10^4$	$0.73 \cdot 10^{-6}$	0.87	$0.1 \cdot 10^7$	$60 \cdot 10^{-7}$	0.50	0.03
Ti50Zr NCZnO	116.23	$10.21 \cdot 10^4$	$2.28 \cdot 10^{-6}$	0.77	$0.32 \cdot 10^7$	$58.4 \cdot 10^{-7}$	0.70	0.02

Tafel plot

Tafel plot diagram for Ti50Zr and coated samples are presented in Figure S4. Using Nova software, parameters like corrosion potential (ε_{corr}) *vs.* Ag/AgCl, 3 M KCl, corrosion current density (j_{corr}) and corrosion rate (mm/year) were obtained and displayed in Table S4.

Also, protection efficiency was calculated using the formula presented in [49]:

$$PE = \frac{i_{corr\,0} - i_{corr\,c}}{i_{corr\,c}} \cdot 100 \quad (2)$$

where $i_{corr\,0}$ is the corrosion current for Ti50Zr substrate and $i_{corr\,c}$ corresponding to modified samples.

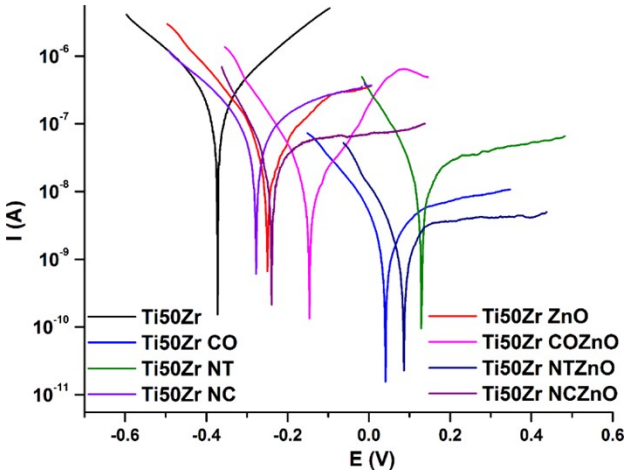

Figure S4. Tafel plot diagram for Ti50Zr substrate and coated samples.

For all coated samples, the corrosion potential is shifted to more electropositive values. Compact oxide, Ti50Zr CO, presents an increased protection efficiency and lower corrosion rate (98%; $2.671 \cdot 10^{-5}$ µm/year) compared to nanotubes, Ti50Zr NT (90 %; $16.0 \cdot 10^{-5}$ µm/year) and nanochannels, Ti50Zr NC (73%; $29.663 \cdot 10^{-5}$ µm/year). Nanochannels being open at bottom have a higher corrosion rate compared to nanotubes. These are also in good correlation with EIS data, where it was observed that R_{ox} is higher for Ti50Zr CO compared to Ti50Zr NT and Ti50Zr NC and $R_{coating}$ is also higher for Ti50Zr NT compared to Ti50Zr NC.

ZnO deposition is lowering the corrosion rate for most samples, Ti50Zr COZnO being an exception already commented in the previous section (EIS). ZnO offers only 57% protection efficiency for Ti50Zr substrate. The better corrosion protection observed for Ti50Zr NT compared to Ti50Zr NC is also reflected for Ti50Zr NTZnO and Ti50Zr NCZnO. Ti50Zr NTZnO presents highest corrosion protection efficiency (99%). Probably the ZnO nanoparticles and thin ZnO coating deposited on nanotube walls can passivate the TiO_2 and ZrO_2 surface defect states.

Table S4. Corrosion parameters from Tafel plots.

Sample	ε_{corr} (V)	j_{corr} (A/cm²)	Corrosion rate (µm/year)	PE (%)
Ti50Zr	-0.372	0.837×10^{-7}	$72.870 \cdot 10^{-5}$	-
Ti50Zr ZnO	-0.249	$0.678 \cdot 10^{-7}$	$44.289 \cdot 10^{-5}$	57
Ti50Zr CO	0.044	$0.028 \cdot 10^{-7}$	$2.671 \cdot 10^{-5}$	98
Ti50Zr COZnO	-0.143	$0.160 \cdot 10^{-7}$	$15.370 \cdot 10^{-5}$	90
Ti50Zr NT	0.133	$0.166 \cdot 10^{-7}$	$16.0 \cdot 10^{-5}$	90
Ti50Zr NTZnO	0.093	$0.023 \cdot 10^{-7}$	$2.218 \cdot 10^{-5}$	99
Ti50Zr NC	-0.277	$0.225 \cdot 10^{-7}$	$29.663 \cdot 10^{-5}$	73
Ti50Zr NCZnO	-0.239	$0.135 \cdot 10^{-7}$	$11.824 \cdot 10^{-5}$	84

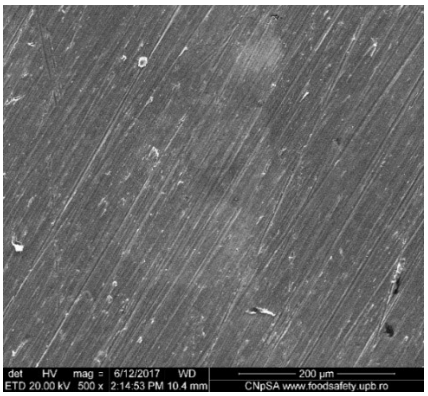

Figure S5. SEM image of plain Ti50Zr.

Table S5. AFM parameters (S_{sk}, S_{ku}, R_{ms}, S_{dr}) for all samples.

Sample	R_{ms} (µm)	S_{dr} (%)	S_{sk}	S_{ku}
Ti50Zr	0.085	0.850	-0.007	2.338
Ti50Zr ZnO	0.929	8.260	-0.031	2.290
Ti50Zr CO	0.050	0.290	-0.063	2.390
Ti50Zr COZnO	0.234	3.980	0.021	2.332
Ti50Zr NT	0.225	2.410	0.029	2.342
Ti50Zr NTZnO	0.204	9.420	0.011	2.333
TI50Zr NC	0.352	17.99	-0.582	4.590
Ti50Zr NCZnO	0.172	34.68	-0.058	2.350

Table S6. Standard deviation (SD) of the AFM parameters (S_{sk}, S_{ku}, R_{ms}, S_{dr}) for all samples.

Sample	SD_{SskAFM}	SD_{SkuAFM}	SD_{RmsAFM} (µm)	SD_{SdrAFM} (%)
Ti50Zr	0.17	1.02	0.02	0.103
Ti50Zr ZnO	0.25	1.25	0.07	2.58
Ti50Zr CO	0.10	0.05	0.01	0.019
Ti50Zr COZnO	0.06	0.14	0.45	1.44
Ti50Zr NT	0.20	0.44	0.04	5.6
Ti50Zr NTZnO	0.45	1.09	0.13	3.34
TI50Zr NC	0.44	0.83	0.02	6.07
Ti50Zr NCZnO	0.21	1.02	0.03	2.54